Initial operation of the NSTX-Upgrade real-time velocity diagnostic

IOP Publishing Plasma Physics and Controlled Fusion

Plasma Phys. Control. Fusion **58** (2016) 125016 (10pp) doi:10.1088/0741-3335/58/12/125016

Initial operation of the NSTX-Upgrade real-time velocity diagnostic

M Podestà and R E Bell

Princeton Plasma Physics Laboratory, Princeton, NJ 08543, USA

E-mail: mpodesta@pppl.gov

Received 5 July 2016, revised 28 September 2016
Accepted for publication 11 October 2016
Published 3 November 2016

Abstract

A real-time velocity (RTV) diagnostic based on active charge-exchange recombination spectroscopy is now operational on the National Spherical Torus Experiment-Upgrade (NSTX-U) spherical torus (Menard *et al* 2012 *Nucl. Fusion* **52** 083015). The system has been designed to supply plasma velocity data in real time to the NSTX-U plasma control system, as required for the implementation of toroidal rotation control. Measurements are available from four radii at a maximum sampling frequency of 5 kHz. Post-discharge analysis of RTV data provides additional information on ion temperature, toroidal velocity and density of carbon impurities. Examples of physics studies enabled by RTV measurements from initial operations of NSTX-U are discussed.

Keywords: NSTX-Upgrade, plasma rotation control, real time rotation measurements, charge exchange recombination spectroscopy

(Some figures may appear in colour only in the online journal)

1. Introduction

Active control of toroidal plasma velocity profile, $v_\phi(R)$ (R is the major radius coordinate), is highly desirable in tokamaks because of the profound effect of rotation on plasma stability. The latter includes stability against magneto-hydro-dynamics (MHD) modes, microturbulence and energetic particle driven instabilities [1, 2]. Following similar research conducted on other tokamaks (see, for example, [3–5]), rotation control[1] [6] is being implemented on the National Spherical Torus Experiment-Upgrade (NSTX-U [7]).

Rotation control is enabled by the availability of both *observers* and *actuators*. Several types of rotation observers can be available on fusion devices. The most commonly used diagnostics rely on the measurement of Doppler-shifted light spectra. By taking into account the observation geometry, the wavelength shift is then converted into velocity (or rotation). Emission in both the visible or x-ray wavelength range has been successfully exploited for velocity measurements, see for example [8–11] and references therein. For control purposes, the *local* velocity—rather than a line integrated value—is preferred. Local velocities are obtained by active charge-exchange spectroscopy using either a diagnostic or heating neutral beam [8].

On NSTX-U, measurements of plasma velocity to feed back on v_ϕ are provided by a dedicated real time velocity (RTV) diagnostic based on active charge exchange recombination spectroscopy. Available actuators are neutral beam injection (NBI) and plasma braking through active magnetic coils. Actions of observers and actuators are coordinated through the NSTX-U plasma control system (PCS [12, 13]).

The RTV system, whose implementation is described in detail in [14], was installed on the NSTX device [15] in 2011. The system was optimized for high throughput and sampling rate up to 5 kHz. Although a sampling rate $\sim$ 1 kHz is adequate for v_ϕ control implementation, higher rates are useful for physics studies requiring measurements of v_ϕ with sub-millisecond time resolution. Initial tests of the RTV system confirmed the achievement of the design specifications, but no RTV operation for plasma discharges was possible because of the beginning of a major upgrade of NSTX. This paper describes the initial operation of the RTV system during the beginning of the first NSTX-U experimental campaign. Examples of research enabled by the new system are provided, focusing on the information that the system can deliver under

[1] The terms *velocity* and *rotation* are used as synonyms throughout the paper since the measurement locations, R_{meas}, are known. Therefore $v_\phi \equiv \omega R_{meas}$, with ω the toroidal rotation.

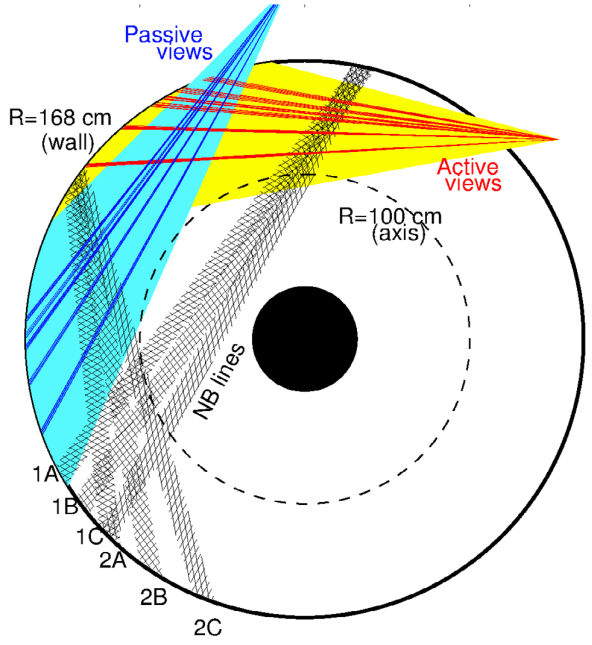

Figure 1. Elevation of NSTX-U showing the layout of the RTV active and background mid-plane views (thick lines). Shaded regions represent the measurement region of the CHERS system. Dashed regions show the paths of the NB lines from first and second NB systems. Each NB line has three sources injecting at different tangency radii, indicated with A, B and C. The magnetic axis is at $R \approx 1$ m. Note that the injection path of the second NBI line intersects the background RTV and CHERS views.

a number of plasma scenarios. The algorithm for real-time v_ϕ control in PCS is still under development, based on the initial results obtained with the new diagnostic. Therefore, examples of actual rotation control will be described in a future dedicated publication.

The remainder of the paper is organized as follows. Section 2 summarizes the experimental setup of NSTX-U and the main parameters of the RTV system. The post-discharge and real-time analysis methods of RTV data are described in section 3, along with a short discussion of the most common issues encountered during the analysis. Section 4 shows examples of the capabilities of the RTV system and the additional information it can reveal of ion velocity and temperature dynamics. Section 6 summarizes the main results of this work and concludes the paper.

2. Experimental setup

2.1. Main NSTX-U parameters

NSTX-U is a spherical torus with major and minor radius $R_0 \approx 1$ m and $a \leqslant 0.6$ m (figure 1). It produces deuterium and helium plasmas with projected toroidal field $\lesssim 1$ T and plasma current up to 2 MA [7], that is an increase of up to a factor 2 from NSTX [15]. Densities are $3\text{–}10 \times 10^{19}$ m^{-3}. Central electron and ion temperature are $T_e \approx T_i \lesssim 2$ keV. Neutral beam (NB) injection is the primary tool for heating and non-inductive current drive. After the upgrade from NSTX, the available power on NSTX-U is $P_{NB} = 12$ MW from two sets of NB injectors. Injection energies are 60–90 keV for deuterium neutrals. Neutral beams are one of the two foreseen actuators for v_ϕ control on NSTX-U. They transfer momentum to the bulk plasma via deposition and ionization of fast neutrals. The second actuator is a set of active magnetic coils installed on the outer vacuum vessel [16]. The coils are mainly used for error field correction during a discharge, but they can also be used to affect plasma rotation [17, 18]. NB and external coils act on different regions of the plasma. Information on v_ϕ from both the core and the edge regions is therefore required to implement flexible velocity profile control schemes [6].

Table 1. Main parameters of the CHERS and RTV systems. Values in parenthesis refer to the background views. For RTV, n_C data are are available only from post-discharge analysis. (Additional RTV views are installed at $R = 137{,}145$ cm [14] but are not used in the present work).

System	CHERS	RTV
Channels	51 (39)	4 (4)
Fibers/channel	2 (1)	8 (7)
Chan. radii (m)	0.85–1.55	1.1,1.25,1.35,1.4
Frame rate (kHz)	0.1	$\leqslant 5$
Measurements	v_ϕ, T_C, n_C	v_ϕ, T_C (n_C)
Monitored line (Å)	C VI, 5290.5	
Dispersion (Å pixel^{-1})	0.21	0.43
Instrum. width (keV)	0.1	0.2

2.2. The RTV diagnostic

Design criteria, implementation and initial tests of the RTV apparatus are described in [14] and summarized below. The main changes since [14] are an improvement of the real-time analysis software, based on actual data from NSTX-U plasmas, and the development of off-line analysis software.

The RTV system complements the main active charge-exchange recombination spectroscopy diagnostic (CHERS [19]) that is routinely used on NSTX-U for measurements of plasma rotation, ion temperature and impurity density. The main parameters of the RTV and CHERS systems are compared in table 1.

For both CHERS and RTV, plasma parameters are inferred from intensity, line broadening and wavelength Doppler shift of the C VI emission line at ≈ 5290.5 Å, corresponding to the $n = 8 - 7$ transition. The diagnostics share two sets of views installed on the mid-plane at two toroidal locations, see figure 1. The two sets are used to separate the *active* charge-exchange C VI emission (originating from the volume illuminated by NB injection) from the background -or *passive*—contribution [19]. The set of background views is toroidally displaced with respect to the active one, to avoid the NB volume and measure only the background emission. Spectra from pairs of active/background views aiming at the same nominal radius are acquired on the same detector to enable real-time data analysis on the acquisition computer.

A main difference from the original setup on NSTX is the presence of a second NB line, whose injection path intersects

the background views (figure 1). Injection from the second NB line compromises the background spectra with spurious and poorly localized *active* emission. All results shown in this paper refer to discharges without injection from the second NB line. Implications for rotation control with the whole set of NB injectors are discussed in sections 3.4 and 5.

3. Analysis of RTV data

An example of spectra measured by the RTV system is shown in figure 2. The figure refers to the L-mode NSTX-U discharge #204202. NB power increased over time from ~ 1.8 MW up to 4.1 MW after $t = 0.5$ s. Data from the $R = 125$ cm active and background views are shown for $t = 0.505$ s. Sampling rate for RTV was 2 KHz for this discharge, compared with the standard 0.1 kHz of the CHERS system.

Figure 2 shows typical features of active charge-exchange spectra on NSTX-U. For sufficiently high NB power, the active component is clearly discernible above the background level. The local temperature $T_C \gtrsim 1.5$ keV, compared to the effective temperature of the edge-localized background emission at ≈ 0.15 keV, results in a clear broadening of the active spectral line. In addition, so-called *plume* emission [20, 21] contaminates the background spectrum. For sufficiently high v_ϕ, plume emission manifests as a tail shifted from the cold, slowly rotating background component with Doppler shift and broadening corresponding to those of the active charge-exchange spectrum.

In the example shown in figure 2, the noise level is comparable for the RTV and CHERS systems. The RTV sampling frequency can be varied to maintain a good signal-to-noise by increasing/decreasing the sampling frequency for discharges with higher/lower injected NB power. For example, the spectrum noise level was quantified for L-mode discharges with only 1 MW of NB power and different values of RTV sampling rate, f_{acq}. For $f_{acq} = 2$ kHz (same as in figure 2), corresponding to an exposure time of 0.5 ms, RTV spectra feature a photon noise level as high as 15–20%. By decreasing f_{acq} to 1 kHz and 0.5 kHz, the noise level decreases to more acceptable levels of 5–10% and $\lesssim 5\%$, respectively. (The original design specification for real-time processing of v_ϕ data was $f_{acq} = 0.33$ kHz, see [14]). Noise level is expected to decrease considerably for more typical levels of NB injected power, $P_{NB} \geqslant 4$ MW.

3.1. Post-discharge analysis

RTV spectra are analyzed after each NB-heated discharge to provide values of plasma rotation, temperature and C VI density at the four RTV measurement locations. The analysis follows the procedure described in [19]. Velocity, temperature and brightness are extracted from a fit of the spectrum for each pair of active/background views. For each view, the fit accounts for intensity corrections, instrumental function and wavelength dispersion, computed from calibrations based on an absolutely calibrated light source and neon glow discharges [14]. Spatial and intensity calibrations are performed both

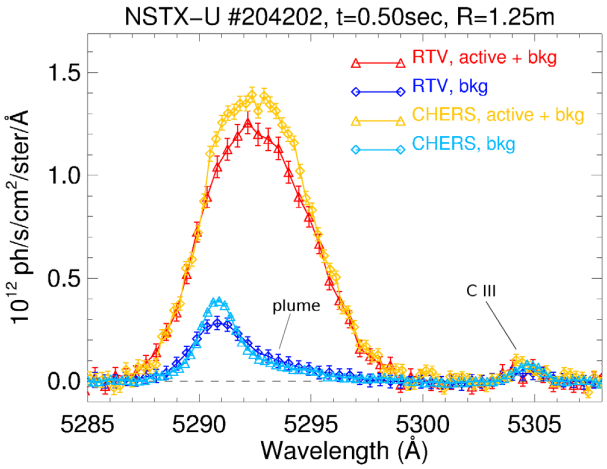

Figure 2. Example of measured brightness spectra for active/background RTV and CHERS views with tangency radius $R \approx 125$ cm. CHERS spectra exhibit sharper features owning to the narrower instrumental width. The line around 5305 Å is C III emission from the plasma edge. The long tail between 5292–5297 Å is plume emission.

before and at the end of each experimental campaign as they require in-vessel access. The raw results from the initial fit are corrected for atomic physics effects, using the available (post-discharge) information on electron density and temperature and magnetic equilibrium. Beam attenuation is also computed at each time to infer the carbon density from the measured brightness of charge-exchange emission. Note that carbon density, n_C, can be inferred from the post-shot analysis but not in the real-time analysis, because it requires knowledge of the electron density profile. The latter is not yet available in real time during a discharge. In addition, electron density is measured at a 60 Hz rate by a Thomson scattering system [22, 23], which is much slower than typical RTV sampling rates.

An example of RTV results for NSTX-U discharge #204202 (see figure 2) is shown in figure 3 for the views aimed at $R = 125$ cm, corresponding to mid-radius for typical NSTX-U plasmas. At the beginning of NB injection, $t \approx 0.12$ s, the plasma is slowly rotating in the counter-current direction. Ion temperature is low, $T_C \approx 0.15$ keV. As momentum and heat are transferred to the plasma through NBI, rotation and ion temperature increase until $t \approx 0.45$ s. At that time, strong MHD instabilities are destabilized, dragging core plasma rotation, which initially saturates and eventually begins to decrease after $t \approx 0.6$ s. Ion temperature, which is less sensitive to the effects of MHD, slowly saturates at values $T_C \approx 1.7$ keV. From figure 3, results from RTV are confirmed by analysis of CHERS data at the nearest CHERS measurement radius. A similar level of agreement is also achieved at the other three measuring locations of RTV, except for n_C that shows discrepancies as large as $\pm 50\%$ between the two systems when multiple discharges and radii are compared. At present, the most likely cause for the discrepancy in n_C appears to be the uncertain absolute intensity calibration for (some of) the RTV channels.

Unlike v_ϕ and T_C results, the inferred n_C from RTV cannot capture rapid changes associated with electron density variations (e.g. affecting NB deposition, or affected by MHD

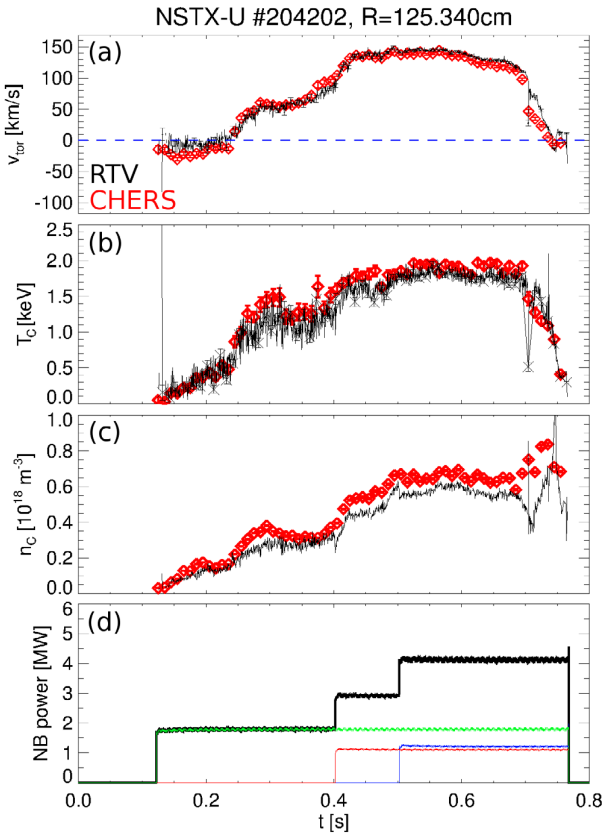

Figure 3. Comparison of (a) velocity, (b) ion temperature and (c) carbon density at $R = 125$ cm from RTV and regular CHERS. (d) Waveforms of the injected NB power from the three sources of NB injection line 1.

instabilities) due to the limited time resolution of Thomson measurements. In the following, only v_ϕ and T_C results are further discussed.

Absolute and relative uncertainties in RTV velocity and temperature results for NSTX-U discharge #204202 are shown in figure 4 for all four measured views. With $f_{acq} = 2$ kHz, uncertainties are significant when only 1.8 MW of NB power is injected at the beginning of the discharge. The addition of 1 MW at $t = 0.4$ s improves the signal-to-noise level, with further improvement as another 1 MW is added at $t = 0.5$ s (as seen in the drop in relative uncertainties, see figures 4(c) and (d)). As expected for L-mode plasmas with core accumulation of carbon, smaller (relative) uncertainties are inferred for the core channels with tangency radius of $R = 112{,}125$ cm. The low carbon density at the edge, $R \gtrsim 135$ cm, results in noisier spectra and therefore larger uncertainties.

Overall, these initial results appear very promising for future RTV measurements, considering (i) the low level of carbon impurities in the discharge shown in figures 3 and 4 (the inferred effective charge based on C VI measurements is $Z_{eff} = 1.2$–1.5), (ii) the relatively high RTV sampling frequency and (iii) the low injected NB power with respect to more standard values $\gtrsim 4$ MW expected for NSTX-U operations.

3.2. Real-time analysis

RTV spectra are analyzed in real-time during a discharge to provide information on velocity (and, possibly, temperature) to PCS. The analysis is a simplified version of the offline analysis described in the previous section. For each view of the two RTV systems, active and background spectra are read out of the detector. Spectra are then corrected by their intensity calibration curve, interpolated on a common wavelength basis and passed to a fitting code to extract v_ϕ and T_C as described in [14].

The fit assumes a gaussian shape for both active and background spectral components. A simplified fit of the plume contribution is also included. The fit returns the wavelength Doppler shift, $\Delta\lambda_D$, and the effective full width at half maximum, w_{eff} for each component. The actual line broadening is estimated by taking into account the (known) instrumental function width, w_{instr}, by setting $w_{true} = \sqrt{w_{eff}^2 - w_{instr}^2}$. Velocity and temperature are then computed from

$$v_\phi(\mathrm{km\ s^{-1}}) = \frac{\bar{c}\ \Delta\lambda_D}{\lambda_{0,C\ VI}} \tag{1}$$

$$T_C(\mathrm{keV}) = \left(\frac{w_{true}}{c_f}\right)^2 \tag{2}$$

where $\bar{c} = 3 \times 10^5\,\mathrm{km\,s^{-1}}$ is the speed of light, $\lambda_{0,C\ VI} = 5290.5$ Å is the C VI rest wavelength and $c_f \approx 3.73$ Å keV^{-2} a temperature conversion coefficient computed for carbon at 5290.5 Å.

A comparison between v_ϕ and T_C results from post-discharge versus real-time analysis of RTV data is shown in figure 5. Considering the simplifications introduced in the real-time analysis, the results compare well. Real-time results have larger uncertainties (figures 5(c)–(f)), deriving from the simplified fit and imperfect removal of spurious contributions to the spectra, e.g. from plume emission.

Overall, the temporal evolution of both v_ϕ and T_C is well recovered in real-time, as required to implement rotation control. At present, real-time results of v_ϕ and associated uncertainty are output as analog voltages [14]. The latter are acquired by PCS and made available for implementing rotation control. Algorithms are under development and will be tested in the near future [6].

3.3. Importance of direct background measurements

A key feature of the RTV system is the direct measurement of background emission by a dedicated set of views that miss the volume illuminated by the first NB line (see figure 1). NB modulation can be used to infer the background spectra for off-line analysis, but the temporal separation of active/passive measurements is not suitable for real-time measurements. For the real-time data processing, however, active and background spectra must be known at each time in order to obtain meaningful measurements.

The importance of measuring and accounting for background emission is illustrated in figure 6. Results from RTV

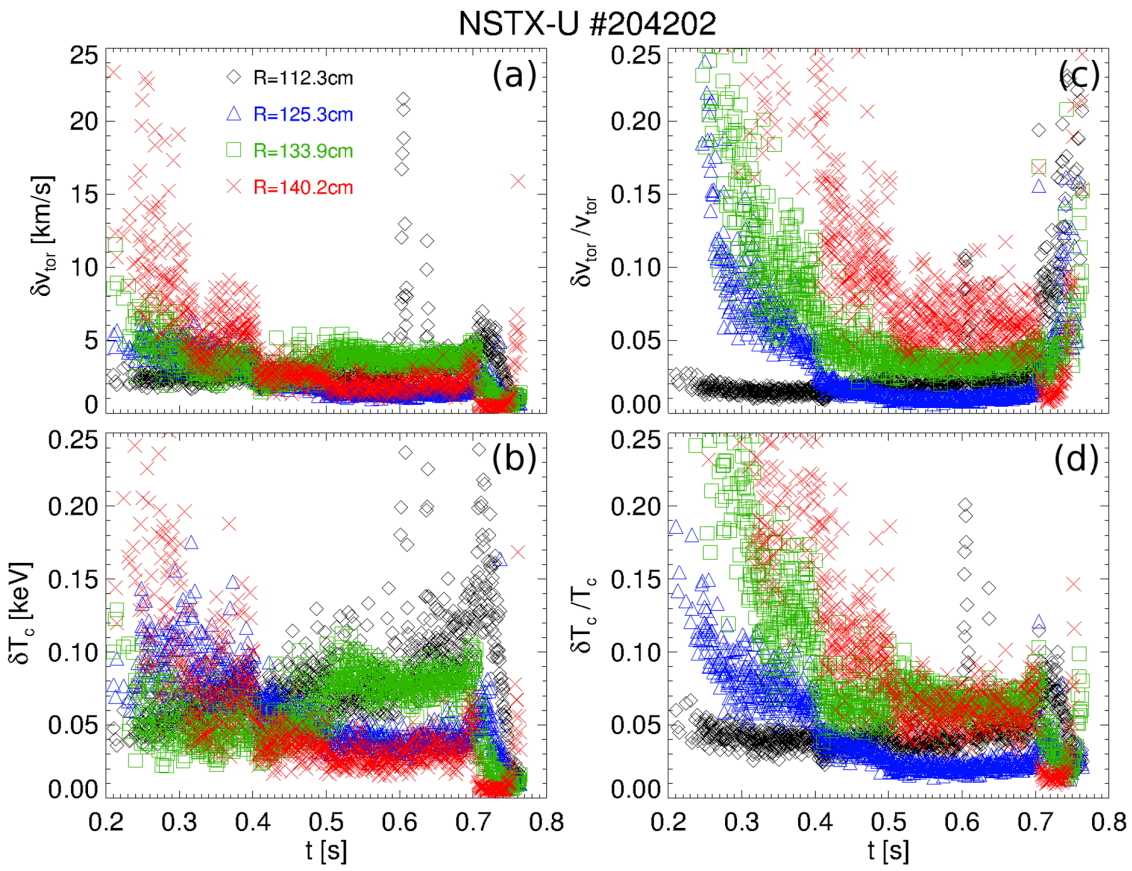

Figure 4. Absolute ((a)–(c)) and relative ((b)–(d)) uncertainties on v_ϕ and T_C results from RTV post-discharge analysis. As time evolves, NB power increases (see figure 3(d)). Colors correspond to different RTV views as per legend in panel (a).

data analysis including background spectra are compared to results that neglect the background. The discharge shown in figure 6 has only 1 MW of injected NB power. Although the target was a L-mode scenario, the plasma actually goes in and out of H-mode about 3 times between 0.6 s and 0.8 s.

Figure 6 clearly shows that accounting for the background emission is crucial for a quantitative analysis of RTV data. Not doing so leads to erroneous results for v_ϕ, T_C and n_C, which can depart by more than a factor 2 from their actual values. The importance of having good background measurements available is further highlighted by scenarios for which those measurements are compromised, as discussed in the next section.

3.4. Contamination of RTV spectra from 2nd NB line injection

As anticipated in the introductory section of this paper, analysis of RTV and CHERS data is compromised when the second NB line is active. As shown in figure 1, background views intercept the volume illuminated by the second NB line over a broad radial range. The resulting *active* (charge-exchange) component contaminates the background spectra. Moreover, an additional plume emission component originates from the second NB line and adds to both active and background views.

An example of raw RTV spectra measured when the second NB line is active is shown in figure 7. The figure shows data from two time points across a turn-off of the second NB line. The two frames are separated by 3 ms, over which it is assumed that plasma and injection parameters of the first NB line do not change significantly. When only the first NB line is active, RTV analysis is possible. Three spectral component are identified (figure 7(a)), namely active, background and plume emission. The three components are then used at the earlier time, when the second NB line is active, to unravel the contaminating emission on the active and background views. As expected, the resulting contamination appears to be composed of multiple components. Looking at the spectrum from the background view, a first component is localized around the rest C VI wavelength at 5290.5 Å and originates from charge-exchange emission within the second NB line volume. A second component is shifted towards longer wavelength (i.e. higher velocity). It is caused by plume emission from both NB lines drifting through the line of sight of the background view. Note that, depending on the velocity profile, the spectral shape of this component is not necessarily a gaussian but can feature significant line distortion [20, 21]. As with the background view, the active view shows an increase in brightness likely caused by additional plume emission from the second NB line.

The example shown in figure 7 demonstrates the challenge of unfolding quantitative information from RTV (and

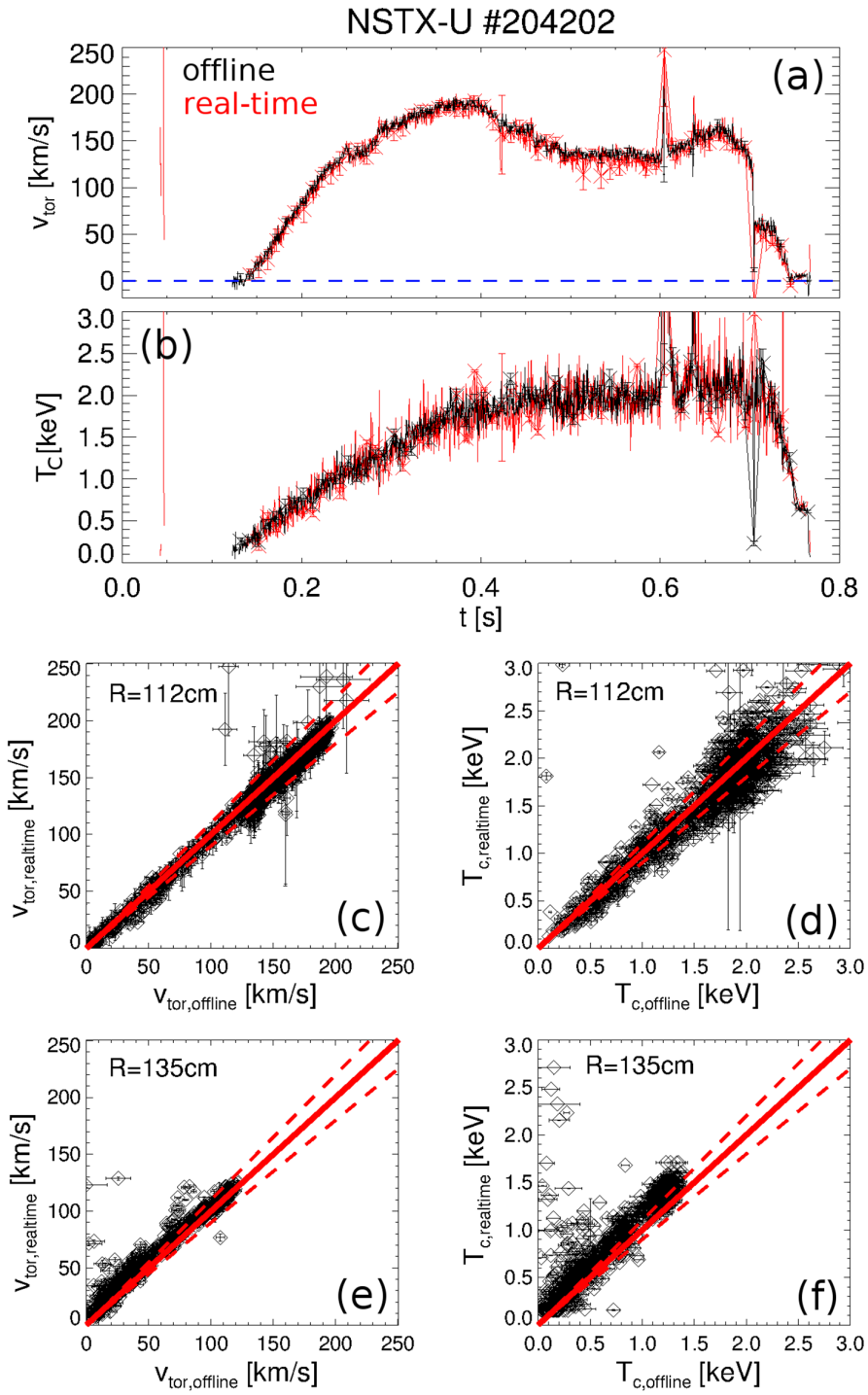

Figure 5. Comparison of (a) velocity and (b) ion temperature from post-discharge and real-time analysis of RTV spectra (shown in black and red, respectively). Direct comparison for v_ϕ and T_C from core ((c)–(d)) and an edge ((e)–(f)) channels shows an overall agreement, although results from the real-time fitting algorithm have larger uncertainties as a result of the simplifications introduced in the fitting algorithm.

CHERS) when the second NB line is active. In typical scenarios the NB sources inject for several tens or hundreds of milliseconds, during which plasma parameters can vary. In this case, it is not possible to simply extrapolates the spectral components from times when only the first NBI is active to times with both NB lines active.

The real-time analysis presents additional complications. Performing such analysis in real time at sufficiently high sampling rate is impossible. Communication with the PCS is unidirectional, from the RTV acquisition and analysis systems to PCS, so no information on which NB source is injecting at each specific time is available in real time. The information

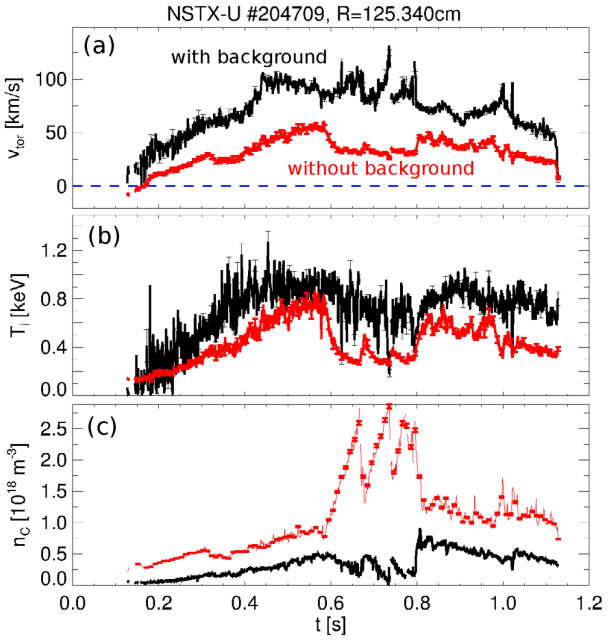

Figure 6. RTV results for (a) velocity, (b) carbon temperature and (c) carbon concentration for NSTX-U discharge #204709 at $R = 125$ cm. Black curves represent the results from regular RTV analysis. Red curves show how the results would change if background emission is not taken into account in the analysis.

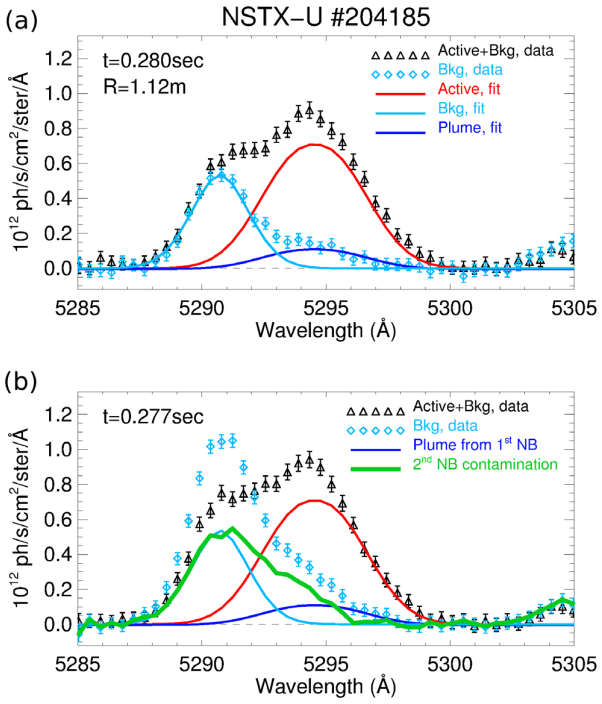

Figure 7. Example of RTV active and background spectra from $R \approx 112$ cm when the second NB line is OFF or ON. RTV sampling frequency is $f_{acq} = 1$ kHz. (a) Spectra without second NB line, separated into their three main components. Injected power from the first NB line is 3 MW. (b) Spectra with ≈ 1.7 MW injected from the second NB line. Results of the fit for charge-exchange, background and plume components are assumed to be the same as in (b). The thick green line is the difference between the spectrum measured by the background view and the background emission from (b).

available from the raw spectra is insufficient to separate the multiple components of the spectra.

4. Examples of physics studies enabled by RTV

The following sections illustrate examples of physics studies enabled by the fast acquisition rate of the RTV system.

The selection of topics is based on results from early operations of NSTX-U during the 2016 experimental campaign.

4.1. Sawteeth and plasma braking effects

The NSTX Upgrade includes a four-fold increase in the available Ohmic flux that drives plasma current. In practical terms, that enables much longer L-mode discharges than were possible on NSTX, resulting in stationary plasma conditions in current flat-top for up to 2 s. These long L-mode discharges are achieved with low NB power, $1 \lesssim P_{NB} \lesssim 3$ MW. The central safety factor is near or below $q = 1$, which triggers sawteeth. RTV results for this scenario are shown in figure 8. Since the sawtooth period is 12–18 ms, CHERS measurements average over most of a sawtooth cycle, and do not capture the details of $v_\phi(t)$ evolution (figure 8(b)). Instead, RTV data at $f_{acq} \geqslant 1$ kHz are capable of measuring velocity (and temperature) evolution throughout the cycle.

Incidentally, pulses of external magnetic perturbations were also applied during the discharge shown in figure 8. The highest amplitude pulse occurs for $1.5 \leqslant t \leqslant 1.75$ s, see figure 8(c). During the pulse, rotation slows down over times scales of tens of milliseconds, which are suitable for both CHERS and RTV systems. In this case, the two systems provide complementary information, with CHERS providing excellent radial resolution and RTV capturing the effects of sawteeth superimposed with magnetic braking (albeit at much reduced spatial resolution).

These stationary L-mode discharges result in a statistically significant set of data to perform conditional average analysis of v_ϕ and T_C evolution during a sawtooth cycle, see figure 9. Data from figure 8 are conditionally averaged for the time window 0.6–1.6 s. For this example, the analysis suggests a different evolution for v_ϕ and T_C under the effects of sawteeth. As expected, momentum (hence v_ϕ) is redistributed from the core region to regions outside the inversion radius (where $q = 1$) located here at $R \approx 125$ cm, resulting in a flattening of $v_\phi(R)$ in the core. The change in central rotation is of the order of 20%. Carbon temperature evolution shows different features, with an apparent inversion radius shifted outward near the $R = 135$ cm RTV channel.

4.2. MHD effects on rotation

MHD and other instabilities driven by energetic particles (EP) are one of the main cause of disruptions and degradation of plasma performance in tokamaks. Characterizing and understanding the effects of instabilities is therefore important to

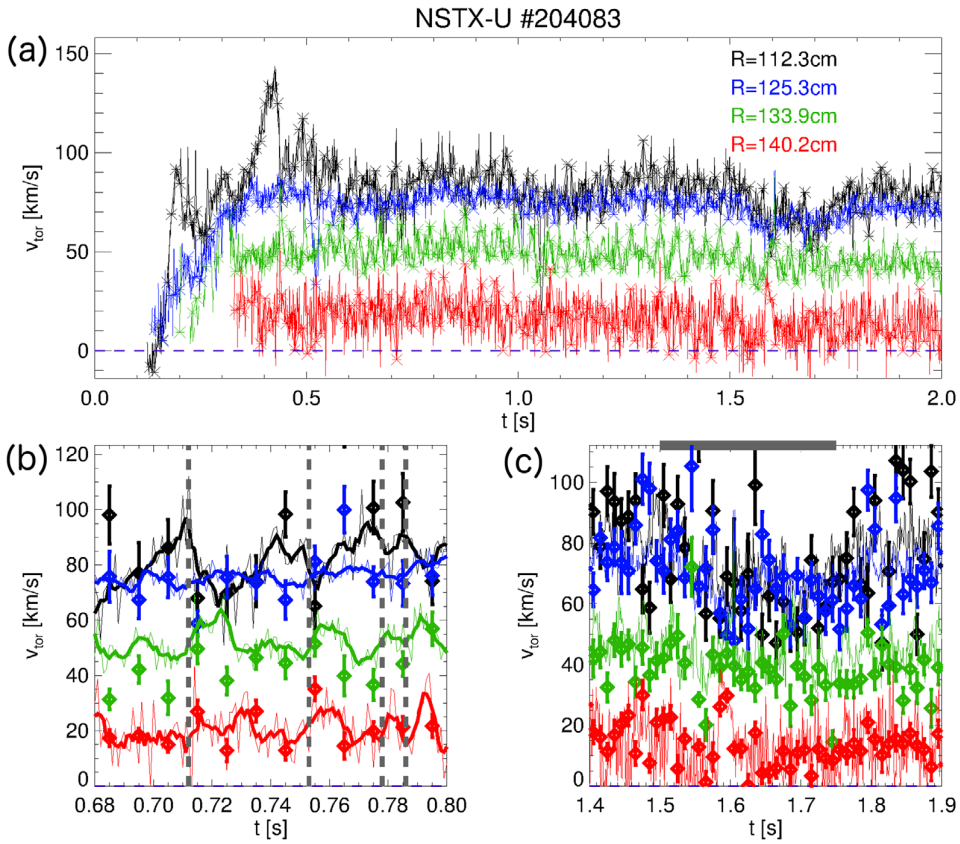

Figure 8. (a) RTV results for plasma velocity at the four measurement radii from a L-mode, sawtoothing plasma with $P_{NB} = 1$ MW. Sawteeth start at $t \approx 0.5$ s. (b) Detail of v_ϕ evolution during sawteeth. Time of sawteeth is indicated by the vertical dashed lines. CHERS results, shown as symbols, are also shown for comparison. (c) Detail of v_ϕ evolution during a pulse of external magnetic coils (duration indicated by the thick gray line), which leads to a decrease—or *braking*—of the central velocity. Channel radii are color coded as per legend in panel (a).

design scenarios that are less prone—or free from—the deleterious effects of perturbations to the plasma equilibrium. Plasma rotation has beneficial effects on instabilities. The availability of velocity data with high temporal resolution is valuable for characterizing the evolution of instabilities and the conditions that can lead to their mitigation or avoidance.

Figure 10 shows a first example of the evolution of toroidal velocity when global MHD modes are destabilized in addition to sawteeth, see figures 8 and 9. As the modes grow after $t = 0.41$ s, the rotation profile flattens inside $R \approx 120$ cm. (No noticeable effects are observed on the $R = 135$ cm view. No measurable charge-exchange signal is available for the outermost view at $R = 140$ cm in this discharge). Sawteeth also begin after 0.45 s and flatten the v_ϕ profile in the core. Eventually, the mode decays at $t \approx 0.55$ s. A constant v_ϕ is maintained by sawteeth until $t \approx 0.78$ s, when MHD is again destabilized and a further decrease in central velocity is measured. When the modes become stable at $t \approx 0.9$ s, a partial recovery of v_ϕ is observed. In this case, the good temporal resolution of the RTV system allows the possibility of separating the effects of different types of disturbances (namely, sawteeth versus MHD modes), which would be more difficult with the lower time resolution of CHERS.

A second example illustrates the velocity evolution when a plasma instability develops and locks to the vacuum vessel wall, causing $v_\phi(R)$ to approach zero across the entire plasma column (figure 11). The effect of such a *locked mode* is first visible on the mid-radius channels, then propagates to the core. Plasma locking at mid-radius happens over a few milliseconds, within a single frame for the CHERS system. The RTV system, though, has enough time resolution to capture the evolution of $v_\phi(t)$. A detailed picture of the effects of the instability can therefore be gathered by combining profile information from CHERS and temporal information from RTV.

5. Routing real-time rotation signals into PCS

PCS is equipped with acquisition modules, deployed around the NSTX-U device and in diagnostic rooms, to acquire analog signals in real time during a discharge [13]. v_ϕ results from RTV are output as re-scaled analog signals from the RTV acquisition systems and sampled by PCS at a 5 kHz rate. Each of the two RTV systems also dispatches a *bit status* signal to indicate to PCS whether the system is available for real-time operations during a discharge. Analog voltages from

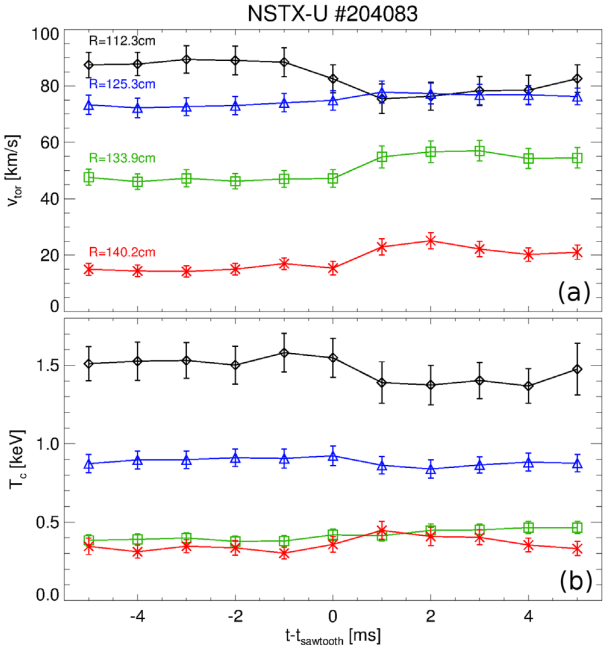

Figure 9. Conditionally averaged (a) velocity and (b) ion temperature at the 4 RTV measuring locations during sawteeth for the L-mode discharge shown in figure 8. About 50 samples from the time window $0.6 \leqslant t \leqslant 1.6$ s are used for the average.

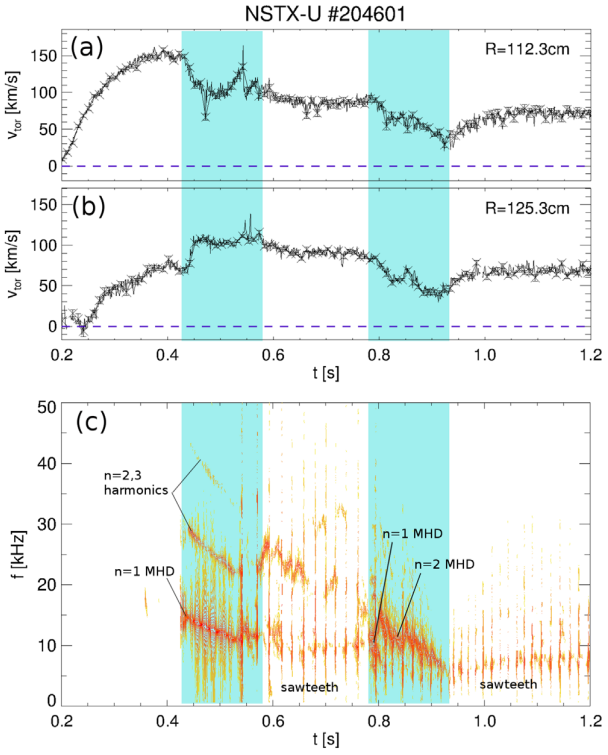

Figure 10. Evolution of v_ϕ in a scenario featuring co-existing sawteeth and internal MHD modes (NSTX-U #204601). ((a)–(b)) v_ϕ measured by RTV at $R = 112$, 125 cm. (c) Spectrum of magnetic fluctuations measured by Mirnov coils installed on the vessel wall. Sawteeth appear as bursty, vertical lines. Toroidal mode number of MHD modes is determined by phase analysis of data from 11 Mirnov coils displaced toroidally.

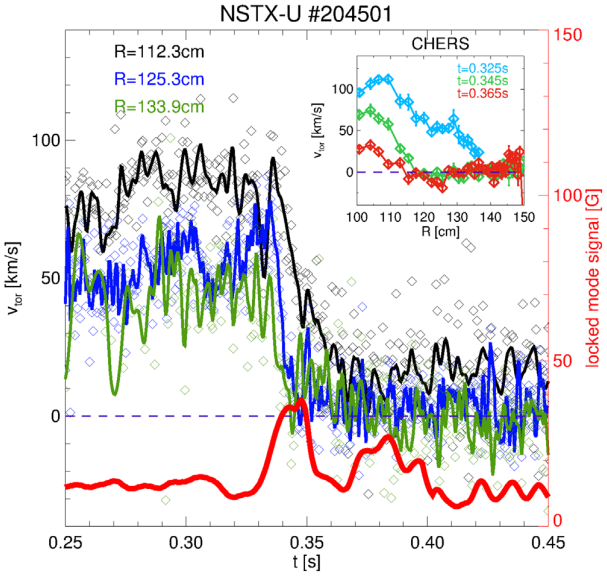

Figure 11. Effect of v_ϕ collapse caused by an internal instability that locks to the vessel wall (NSTX-U #204501). Symbols represent RTV measurements at three radii. Thick lines are a smooth fit of the data. The thick, red line shows the measured amplitude of the *locked mode*, whose amplitude spikes after $t \approx 0.33$ s causing the reduction in v_ϕ. The plasma disrupt shortly after $t \approx 0.45$ s. The inset shows CHERS radial profiles before, during and after the maximum mode activity.

RTV are re-scaled to fit within a $[-10, +10]$ V range. Scaling coefficients (and measurement locations) are stored into the MDSplus tree prior to a discharge and reloaded by PCS to convert the analog inputs into physical units. NB power threshold values are set through the PCS software to flag acceptable RTV data depending on which NB line is active during a discharge. As a default, data are flagged as unreliable whenever the second NB line is injecting.

At present, signals are acquired by PCS but no algorithm has been developed yet to act on plasma rotation through the available actuators. Work is in progress to develop a physics-based model that can then be implemented in PCS in the near future [6].

6. Summary

A new diagnostic for fast measurements of toroidal rotation and temperature of carbon ions has been installed and tested on NSTX-U. The system can deliver v_ϕ and T_C on a sub-millisecond time scale. Post-discharge analysis enables the study of transient phenomena, e.g. associated with MHD perturbations or external perturbations through magnetic coils. These new results complement previously available data from the NSTX-U CHERS system, which features high spatial resolution but slower time resolution (10 ms sampling rate). The system has been developed to provide data in real-time to the NSTX-U plasma control system, as required for the future implementation of toroidal velocity feed-back control schemes. Although the present RTV system is based on active charge-exchange recombination spectroscopy, the same

approach described in this work could be extended to other diagnostics, such as x-ray spectrometers. The main advantage of exploiting a x-ray-based system for real time velocity measurements would be the availability of data without the need of NB injection from either a heating or diagnostic neutral beam, although an inversion is required to infer local velocities [10].

Acknowledgments

Discussions and support from the NSTX-U PCS group is kindly acknowledged. Importing real-time signals from the RTV systems into PCS has been made possible by the work of J E Lawson, K Lamb, K Erickson, R Rosenblatz and S P Gerhardt (PPPL). This work was supported by the US DoE Office of Science—Fusion Energy Sciences, under Contract Number DE-AC02-09CH11466. NSTX-U at Princeton Plasma Physics Laboratory (Princeton University, New Jersey—USA) is a DOE Office of Science User Facility. The digital data for this paper can be found from http://arks.princeton.edu/ark:/88435/dsp011v53k0334.

References

[1] Berkery J W, Sabbagh S A, Betti R, Hu B, Bell R E, Gerhardt S P, Manickam J and Tritz K 2010 *Phys. Rev. Lett.* **104** 035003
[2] Terry P W 2000 *Rev. Mod. Phys.* **72** 109
[3] Heesterman P J L, Sall I, Giraud C, Zastrow K D, Meigs A, Felton R and Joffrin E 2003 *Rev. Sci. Instrum.* **74** 1783
[4] Yoshida M, Sakamoto Y, Sueoka M, Kawamata Y, Oyama N, Suzuki T, Kamada Y and The JT-60 Team 2009 *Fusion Eng. Des.* **84** 2206
[5] Scoville J T, Humphreys D A, Ferron J R and Gohil P 2007 *Fusion Eng. Des.* **82** 1045
[6] Goumiri I R, Rowley C W, Sabbagh S A, Gates D A, Gerhardt S P, Boyer M D, Andre R, Kolemen E and Taira K 2016 *Nucl. Fusion* **56** 036023
[7] Menard J E *et al* and NSTX Team 2012 *Nucl. Fusion* **52** 083015
[8] Thomas D M 2012 *Phys. Plasmas* **19** 056118
[9] Stratton B C, Bitter M, Hill K W, Hillis D L and Hogan J T 2008 *Fusion Sci. Technol.* **53** 431
[10] Reinke M L *et al* 2012 *Rev. Sci. Instrum.* **83** 113504
[11] Rice J E 2016 *Plasma Phys. Control. Fusion* **58** 083001
[12] Mastrovito D, Gates D, Gerhard S P, Lawson J, Ludescher-Furth C and Marsala R 2010 *Fusion Eng. Des.* **85** 447
[13] Erickson K G, Gates D A, Gerhardt S P, Lawson J E, Mozulay R, Sichta P and Tchilinguirian G J 2014 *Fusion Eng. Des.* **89** 853
[14] Podestà M and Bell R E 2012 *Rev. Sci. Instrum.* **83** 033503
[15] Ono M *et al* and NSTX Team 2000 *Nucl. Fusion* **40** 557
[16] Sabbagh S A *et al* and The NSTX Research Team 2004 *Nucl. Fusion* **44** 560
[17] Zhu W *et al* 2006 *Phys. Rev. Lett.* **96** 225002
[18] Sabbagh S A *et al* 2010 *Nucl. Fusion* **50** 025020
[19] Bell R E, Andre R, Kaye S M, Kolesnikov R A, LeBlanc B P, Rewoldt G, Wang W X and Sabbagh S A 2010 *Phys. Plasmas* **17** 082507
[20] Fonck R J, Darrow D S and Jaehnig K P 1984 *Phys. Rev.* A **29** 3288
[21] Bell R E 2006 *Rev. Sci. Instrum.* **77** 10E902
[22] LeBlanc B P, Bell R E, Johnson D W, Hoffman D E, Long D C and Palladino R W 2003 *Rev. Sci. Instrum.* **74** 1659
[23] Diallo A, LeBlanc B P, Labik G and Stevens D 2012 *Rev. Sci. Instrum.* **83** 10D532